SHOCK INDUCED STRUCTURAL RESPONSE

Jose Gonzalo Gallo

NAVAL POSTGRADUATE SCHOOL
Monterey, California

THESIS

SHOCK INDUCED STRUCTURAL RESPONSE

by

Jose Gonzalo Gallo

March 1978

Thesis Advisor: R. E. Newton

SECURITY CLASSIFICATION OF THIS PAGE (When Data Entered)

REPORT DOCUMENTATION PAGE

READ INSTRUCTIONS BEFORE COMPLETING FORM

1. REPORT NUMBER	2. GOVT ACCESSION NO. / 3. RECIPIENT'S CATALOG NUMBER
4. TITLE (and Subtitle): Shock Induced Structural Response	5. TYPE OF REPORT & PERIOD COVERED: Engineer's Thesis; March 1978
	6. PERFORMING ORG. REPORT NUMBER
7. AUTHOR(s): Jose Gonzalo Gallo	8. CONTRACT OR GRANT NUMBER(s)
9. PERFORMING ORGANIZATION NAME AND ADDRESS: Naval Postgraduate School, Monterey, California 93940	10. PROGRAM ELEMENT, PROJECT, TASK AREA & WORK UNIT NUMBERS
11. CONTROLLING OFFICE NAME AND ADDRESS: Naval Postgraduate School, Monterey, California 93940	12. REPORT DATE: March 1978
	13. NUMBER OF PAGES: 59
14. MONITORING AGENCY NAME & ADDRESS(if different from Controlling Office): Naval Postgraduate School, Monterey, California 93940	15. SECURITY CLASS. (of this report): Unclassified
	15a. DECLASSIFICATION/DOWNGRADING SCHEDULE

16. DISTRIBUTION STATEMENT (of this Report)

Approved for public release; distribution unlimited.

17. DISTRIBUTION STATEMENT (of the abstract entered in Block 20, if different from Report)

18. SUPPLEMENTARY NOTES

19. KEY WORDS (Continue on reverse side if necessary and identify by block number)

Finite element
Pressure resolution
Radiation boundary condition
Failure boundaries
Underwater shock

20. ABSTRACT (Continue on reverse side if necessary and identify by block number)

An infinitely long, ring-stiffened, submerged, elastic cylinder having uniformly spaced elastic bulkheads is the structure considered. Loading is applied by a plane acoustic shock wave with front parallel to the cylinder axis. Dynamic pressure in the fluid is resolved into a free-field incident part and a scattered part. Structural response and scattered pressure in the surrounding fluid are found using finite element modeling of structure and fluid. Introduction of Fourier series makes the fluid

DD FORM 1 JAN 73 1473 EDITION OF 1 NOV 65 IS OBSOLETE
S/N 0102-014-6601 |
(Page 1)

SECURITY CLASSIFICATION OF THIS PAGE (When Data Entered)

region mathematically two-dimensional. A radiation, or non-reflecting, condition at the outer boundary of the fluid region is shown to give good results. A parametric study is made of effects of shock pulse rise time and duration on structural response. Results are presented as combinations of shock pressure and submergence pressure just sufficient to induce structural failure.

Approved for public release; distribution unlimited

Shock Induced Structural Response

by

Jose Gonzalo Gallo
Lieutenant, Peruvian Navy

Submitted in partial fulfillment of the
requirements for the degrees of

MECHANICAL ENGINEER

and

MASTER OF SCIENCE IN MECHANICAL ENGINEERING

from the

NAVAL POSTGRADUATE SCHOOL
March 1978

ABSTRACT

An infinitely long, ring-stiffened, submerged, elastic cylinder having uniformly spaced elastic bulkheads is the structure considered. Loading is applied by a plane acoustic shock wave with front parallel to the cylinder axis. Dynamic pressure in the fluid is resolved into a free-field incident part and a scattered part. Structural response and scattered pressure in the surrounding fluid are found using finite element modeling of structure and fluid. Introduction of Fourier series makes the fluid region mathematically two-dimensional. A radiation, or non-reflecting, condition at the outer boundary of the fluid region is shown to give good results. A parametric study is made of effects of shock pulse rise time and duration on structural response. Results are presented as combinations of shock pressure and submergence pressure just sufficient to induce structural failure.

TABLE OF CONTENTS

LIST OF TABLES

LIST OF FIGURES

ACKNOWLEDGEMENT

The author wishes to express his deep appreciation to Dr. Robert E. Newton, Professor of Mechanical Engineering, for his guidance and help throughout this investigation. A special note of gratitude is extended to the staff of the W. R. Church Computer Center of the Naval Postgraduate School.

Finally, the author thanks his family, Ana Maria, Jose Gustavo, Maria Alejandra and Ricardo Alfonso for their love and patience.

I. INTRODUCTION

This investigation is the third in a sequence of finite element studies of fluid-structure interaction. The initial study was by Atchison [1] and the second by Newton and Atchison [2]. The system considered, as in the earlier studies, is a submarine subjected to a shock wave resulting from an underwater explosion. The submarine is modeled as a ring-stiffened cylinder of infinite length with equally spaced elastic bulkheads. The shock wave is a plane acoustic wave with front parallel to the longitudinal axis of the cylinder. The structure-fluid equations are coupled by terms resulting from dynamic interaction at the interface boundary.

A. PRIOR STUDIES

It is shown by both authors in references [1] and [2] that the three-dimensional problem may be resolved into two-dimensional subproblems, acoustic wave propagation and transient response of a submerged structure, using the finite element method.

Acoustic wave propagation and spatial fluid discretization are presented in [1]. The superposition theorem, which permits the rigid body pressure distribution to be obtained from a two-dimensional analysis is also presented in [1].

A refined structural model is used in [2]. In this paper, the circumferential variations of fluid pressures and structure displacements are represented by Fourier expansions. Fluid pressures, structural deflections, shell and ring stresses are tabulated for each harmonic through n=4. Extreme stresses resulting from superposition of harmonic

contributions are given also. Two separate failure criteria are used to determine critical combinations of submergence pressure and shock pressure. The first of these utilizes limit analysis to evaluate combined effects of longitudinal and axial stress in the shell wall at a bulkhead. The second postulates that shell collapse will occur when the von Mises yield condition is satisfied away from the bulkhead.

B. PRESENT STUDY

In the present study the need for a separate solution of the acoustic propagation is eliminated, thus effecting a significant reduction in computation. This improvement is made by dealing separately with the incident shock pressure - an entity which is unaffected by the presence of the structure. The remainder of the dynamic fluid pressure (called the "scattered" pressure) is represented in the finite element modeling of fluid-structure response. As in [2], the azimuthal variation of fluid pressure and structural displacement are represented by trigonometric series so that the fluid region modeled is mathematically two-dimensional.

A further improvement introduced here is the imposition of a radiation boundary condition at the cylindric outer boundary of the fluid. Although this condition is necessarily approximate, it is found to reduce significantly the effects of boundary reflections on structural response.

A systematic study is made of the effects of shock pulse duration and rise time on structural response. Results are presented in the form of critical combinations of shock pressure and submergence pressure just sufficient to induce structural failure.

II. WAVE PROPAGATION

A. PRESSURE RESOLUTION

A submerged structure subjected to an underwater shock wave experiences, at a given time, a total dynamic pressure which can be considered to have three components

$$p = p_i + p_R + p_r \tag{1}$$

where

p is the total dynamic pressure in the fluid,

p_i is the pressure due to the incident wave, considering the structure absent,

p_R is the pressure due to the reflected wave, considering no structural deflection,

p_r is the pressure radiated by the structure due to structural deflection.

There are two useful combinations of these pressures for purposes of analysis. Consider first

$$p_{rig} = p_i + p_R \tag{2}$$

where p_{rig} represents the total dynamic pressure field with a rigid structure. Next consider

$$p_s = p_R + p_r \tag{3}$$

where p_s represents the scattered pressure, which includes both reflected and radiated parts.

Instead of considering the total dynamic pressure to be the sum of p_{rig} and p_r as in [1] and [2], the resolution

$$p = p_i + p_s \tag{4}$$

will be used. This resolution has been employed widely in similar problems, e.g., by Mindlin and Bleich [3], Geers [4] and Everstine [5].

The discretized equations for the structure and fluid given in [1] and [2] are

$$\underline{M}\,\ddot{\underline{\delta}} + \underline{K}\,\underline{\delta} = \underline{L}\,\underline{p} \tag{5}$$

$$\underline{Q}\,\ddot{\underline{p}} + \underline{D}\,\dot{\underline{p}} + \underline{H}\,\underline{p} = -\rho\,\underline{L}^T\,\ddot{\underline{\delta}} \tag{6}$$

where $\underline{\delta}$ is a column vector of structural nodal displacements and $\underline{p}$ is a column vector of fluid nodal pressures. $\underline{M}$, $\underline{K}$, $\underline{Q}$, $\underline{D}$ and $\underline{H}$ are symmetric coefficient matrices, $\underline{L}$ is a matrix describing coupling at the structure-fluid interface, and ρ is the fluid density. Superior dots denote time derivatives and superscript T denotes transposition.

Considering first the incident pressure only, a time-dependent column vector $\underline{f}$ is added to correct for the unsatisfied boundary condition at the fluid-structure interface. It is required that

$$\underline{Q}\,\ddot{\underline{p}}_i + \underline{D}\,\dot{\underline{p}}_i + \underline{H}\,\underline{p}_i = \underline{f} \tag{7}$$

Considering next the scattered pressure, it is required that

$$\underline{Q}\,\ddot{\underline{p}}_s + \underline{D}\,\dot{\underline{p}}_s + \underline{H}\,\underline{p}_s = -\rho\,\underline{L}^T\,\ddot{\underline{\delta}} - \underline{f} \tag{8}$$

The equation for the structure (5) becomes

$$\underline{M}\,\ddot{\underline{\delta}} + \underline{K}\,\underline{\delta} = \underline{L}\,\underline{p}_i + \underline{L}\,\underline{p}_s \tag{9}$$

Therefore, equations (7), (8) and (9) are the new equations for the complete elasto-hydrodynamic problem formulated by Atchison [1] and Newton and Atchison [2].

Rather than use equation (7) to find $\underline{f}$, the relation between the incident pressure and the fluid particle velocity normal to the boundary may be used.

Consider a plane wave traveling in the negative x-direction. The free-field incident pressure is given by

$$p_i = g(x + ct) \tag{10}$$

where c is the acoustic velocity of propagation. Fig. 1 represents the wave front.

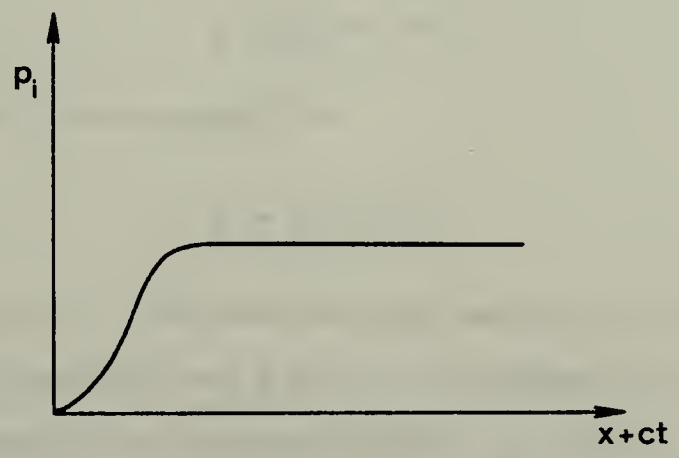

Fig. 1. Wave front.

Applying Newton's second law to a fluid particle, it can be shown that the fluid acceleration is given by

$$\dot{v} = -\frac{1}{\rho}\frac{\partial p_i}{\partial x} = -\frac{g'}{\rho} \tag{11}$$

However

$$\dot{p}_i = \frac{\partial p_i}{\partial t} = g'c$$

Therefore, in (11)

$$\dot{v} = -\frac{1}{\rho c}\dot{p}_i \tag{12}$$

Formula (12) gives the relation between the incident pressure and the fluid particle velocity. The complete problem now is reduced to solving the set of linear equations given by (8) and (9) using the result established by equation (12).

Fourier representations are employed in deriving the discretized counterparts of equations (8) and (9) for each pressure harmonic and displacement harmonic. Because both the structure and the fluid region are axisymmetric, there is no interharmonic coupling.

Therefore, for the structure displacement, let

$$\underline{\delta} = \underline{\delta}_n \cos n\theta \tag{13}$$

and, for the fluid pressure, let

$$\underline{p} = \underline{p}_n \cos n\theta \tag{14}$$

where $n=0,1,2,\ldots$ and summation with respect to n is implied.

For each Fourier order n there is a separate pair of equations (8) and (9) governing the corresponding pair $\underline{\delta}_n$ and $\underline{p}_n$ of displacement and pressure vectors. The coefficient matrices of these equations are order-dependent. Formulas for these matrices are given in Appendix A.

B. RADIATION BOUNDARY CONDITION

Finite element modeling of infinite regions always requires some strategem to avoid significant errors due to substitution of a finite

region. In most static problems and some steady-state dynamic problems it suffices to place the boundaries "far enough" from the region of interest. This scheme is also applicable to the present problem featuring wave propagation in the fluid. Here the requirement of "far enough" is satisfied if waves traveling from structure to outer boundary and back to the structure arrive after the occurrence of maximum stresses in the structure. Meeting this requirement led, in the present application, to a finite element model in which over 80 percent of the degrees of freedom represent fluid pressures.

An alternate means for simulating an infinite region utilizes a radiation, or non-reflecting, condition at the outer boundaries. Such a condition was first proposed by Zienkiewicz and Newton [6] in a form which is exact for plane waves normally incident upon the boundary. Chenault successfully employed the condition in a study of two-dimensional added mass and damping [7]. Dean constructed and successfully demonstrated an extension to spherically spreading waves [8]. For both plane and spherical waves the corresponding non-reflecting conditions are exact, but no such result is possible for two-dimensional (cylindric) spreading. Despite the necessity for approximation, Bai constructed and used a radiation condition for two dimensions [9]. An extension of Bai's scheme is developed in the section entitled "Two-Dimensional Analysis".

C. ONE-DIMENSIONAL ANALYSIS

A one-dimensional analysis using the new pressure resolution has been done in order to compare new results with those previously obtained by Atchison [1].

The region considered is a semi-infinite fluid strip of unit cross sectional area. Through this region a shock wave of known shape is

propagating. The semi-infinite strip is modeled with a one degree of freedom structure at one end and the radiation boundary condition is applied at the other end.

The results obtained were compared with those obtained by using CSMP (continuous system modeling program). Good agreement was found. Accordingly, the Houbolt integration method [10], the linear element, and the restrictions for node spacing and time step as used in [1] and [2] were found to give excellent results when used with the new pressure resolution.

D. TWO-DIMENSIONAL ANALYSIS

1. Boundary Conditions

A non-reflecting or radiation boundary condition is presented and used with this fluid-structure investigation.

If it is wished to let a plane wave traveling in the positive x-direction pass out of the region being investigated, the condition required is

$$\frac{\partial p}{\partial x} = -\frac{1}{c}\dot{p} \tag{15}$$

In dealing with two-dimensional problems, the axisymmetric approximation proposed by Bai [9] is adapted. The (scattered) pressure distribution for a wave moving in the positive r-direction is assumed to be described by

$$p_s = r^{-1/2} g_n(r-ct)\cos n\theta \tag{16}$$

where, as before, there is summation with respect to index n.

The boundary condition imposes a requirement on the normal derivative of the pressure at the boundary. The partial derivative is calculated from equation (16) as

$$\frac{\partial p_s}{\partial r} = -\frac{1}{2} r^{-3/2} g_n(r-ct) \cos n\theta + r^{-1/2} g_n'(r-ct) \cos n\theta \qquad (17)$$

Also

$$\dot{p}_s = \frac{\partial p_s}{\partial t} = r^{-1/2} g_n'(r-ct) \cos n\theta (-c)$$

or

$$\frac{\dot{p}_s}{c} = -r^{-1/2} g_n'(r-ct) \cos n\theta$$

Therefore, equation (17) may be rewritten as

$$\frac{\partial p_s}{\partial r} = -\frac{p_s}{2r} - \frac{\dot{p}_s}{c} \qquad (18)$$

This formula will be introduced as the radiation boundary condition for the solution of the interaction problem. Data concerning the usefulness of this approximation are given in the section titled Results.

2. Fourier Analysis

It is required, in order to solve equations (8) and (9), to know both the incident pressure and the normal component of the fluid acceleration at the structure-fluid interface.

The pressure-time history of the cubic ramp-box wave used may be represented as shown in Fig. 2, where τ_r is the pulse rise time, τ_d is the pulse duration and τ_s is the subsidence time.

For a given incident pressure wave, characterized by rise time, pulse duration, subsidence time, acoustic velocity and fluid density, it is required to find Fourier components for the incident pressure and

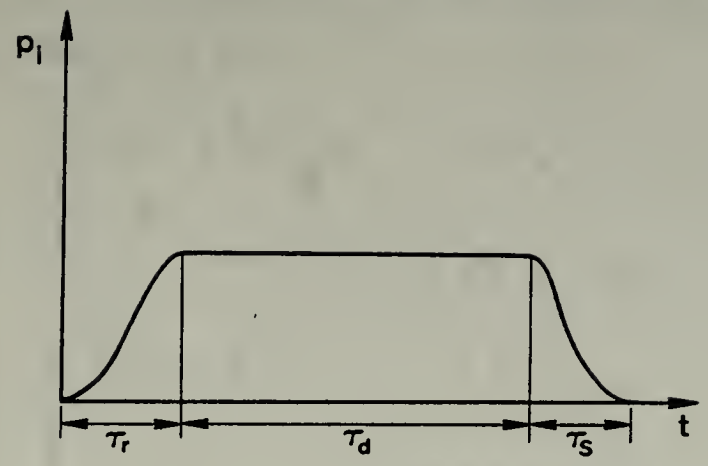

Fig. 2. Pressure-time history of a cubic ramp-box wave.

fluid acceleration at the shell surface using a chosen time step h. These Fourier components are needed for as many time steps as are used in solving the fluid-structure equations.

Basic parameters for the Fourier analysis are shown in Fig. 3.

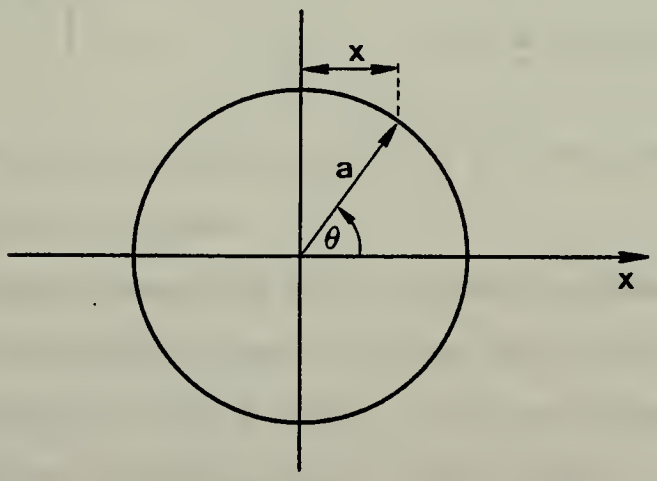

Fig. 3. Parameters used in Fourier analysis.

For the cubic wave front, pressure and pressure derivative formulas are derived by Atchison in [1]

$$p_i = \begin{cases} (3\zeta^2 - 2\zeta^2)p^* , & t < \tau_r \\ p^* , & \tau_r \leq t \leq (\tau_r + \tau_d) \end{cases} \tag{19}$$

$$\dot{p}_i = \begin{cases} \frac{6p^*}{\tau_r}(\zeta - \zeta^2) , & t < \tau_r \\ 0 , & \tau_r \leq t \leq (\tau_r + \tau_d) \end{cases} \tag{20}$$

where $\zeta = \frac{t}{\tau_r}$ and p^* is the shock pressure.

The subsidence is described by the same kind of cubic transition as the rise.

Relations for the normal (perpendicular) component $\dot{v}_p$ of the fluid acceleration can be derived using equations (12) and (19). Thus

$$\dot{v}_p = \begin{cases} \frac{6\ p^*}{\rho c\ \tau_r}(\zeta - \zeta^2)\cos\theta , & t < \tau_r \\ 0 , & \tau_r \leq t \leq (\tau_r + \tau_d) \end{cases} \tag{21}$$

Therefore, equations (19) and (21) are used as basic formulation for the Fourier analysis.

Fourier components for the incident pressure and fluid acceleration are calculated for each time step using 24 intervals over the cylinder from $\theta = 0°$ to $\theta = 180°$. It is not necessary to include values of θ from 180° to 360° because of symmetry about $\theta = 0°$.

For the incident pressure coefficients

$$A_o = \frac{1}{N}\sum_{J=0}^{N} w_J \, p_{i_J} \qquad N = 24 \qquad (22)$$

$$n = 1,2,3,4$$

$$A_n = \frac{2}{N}\sum_{J=0}^{N} w_J \, p_{i_J} \cos n\theta_J$$

where $w_o = w_N = 1/2$ and all other $w_J = 1$.

For the fluid normal acceleration components

$$B_o = \frac{1}{N}\sum_{J=0}^{N} w_J \, \dot{v}_{p_J} \qquad N = 24 \qquad (23)$$

$$n = 1,2,3,4$$

$$B_n = \frac{2}{N}\sum_{J=0}^{N} w_J \, \dot{v}_{p_J} \cos n\theta_J$$

Required values of p_i and $\dot{v}_p$ are found from equations (19) and (21).

New Fourier resolutions are required when any characteristic time of the shock pulse is changed.

III. STRUCTURAL RESPONSE

A. STRUCTURAL MODEL

A refined model is used for the structure. A total of eight structural elements and 27 structural degrees of freedom per Fourier component represent the final mesh and it is identical with the one utilized by Newton and Atchison [2].

As described in [2], the structure is a ring-stiffened elastic shell of infinite length with elastic bulkheads at spacing 2L. Fig. 4 shows a cross-section of the repeating length of structure and the associated fluid region.

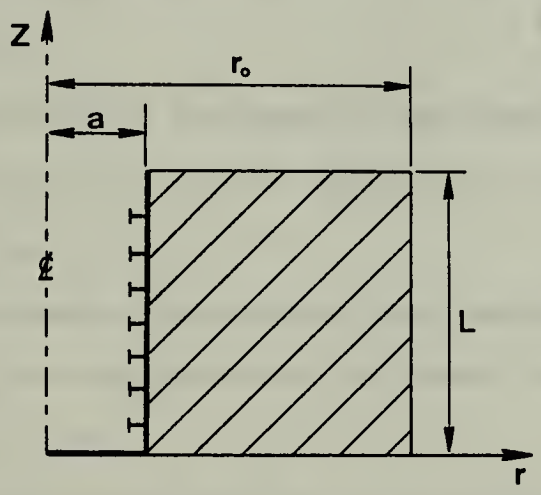

Fig. 4. Region represented by finite element model.

It is assumed that the plane of a bulkhead, z=0, and the plane midway between bulkheads, z=L, are planes of symmetry for the structure and the response displacements.

As in reference [2], the effects of the stiffening rings are included by treating the shell as orthotropic. Stress calculations take

into account the geometry of the rings. The effective shell thickness in the circumferential direction includes a contribution by the rings.

The bulkheads furnish elastic restraint against radial displacement of the shell. This is accomplished by treating the bulkhead as a diaphragm of uniform thickness.

As developed in reference [2] a geometric stiffness matrix modifies the structural stiffness. It considers the effects of the membrane compressive stresses of the axisymmetric mode acting to amplify deflections in the higher harmonics (n>1).

Further information concerning the structural model is given in reference [2]. Details concerning application of Fourier series to analysis of axisymmetric shells are given by Grafton and Strome [11].

B. FLUID MODEL

As indicated in Fig. 4 the length of the fluid region is one-half of the bulkhead spacing, its inner radius is the shell radius "a", and the outer radius is r_o.

Rectangular elements having corner nodes and linear shape function are used. Along the fluid-structure interface a fluid node is located at each structural node.

The radiation boundary condition as developed previously is applied at the outer radius r_o. For the purpose of studying the effectiveness of the radiation boundary condition, the same combination of pulse parameters and submergence pressure has been employed using a=5 meters and a sequence of values of r_o from 8.15 meters to 17.6 meters.

In finding critical combinations of shock and submergence pressure to induce structural failure two different meshes are utilized. In each

case the fluid region has inner radius a = 5 meters and outer radius r_o = 16.025 meters. The first mesh has 90 fluid elements and 120 fluid nodes and each element has a thickness (radial) of 0.525 meters. The second has 174 fluid elements and 225 fluid nodes with element thickness 0.2625 meters. The latter mesh is used when the rise time of the wave front is small in order to meet the restriction given by Atchison [1] as

$$s \leq \frac{c\tau_r}{2} \tag{24}$$

where s is the node spacing. Two different time steps are employed depending on the size of the mesh. For the finer mesh a time step of 0.1 milliseconds is used. For the coarser mesh the time step is 0.3 milliseconds.

C. SOLUTION TECHNIQUE

The solution process is very similar to the one used by Newton and Atchison [2].

There is a separate solution for each of the five harmonics considered (from n=0 to n=4). Once the solution for the first harmonic is completed, the solution for the second starts and the other harmonics follow in order.

Fourier components for the incident pressure and normal fluid acceleration are introduced as input for each solution.

For any harmonic the procedure employed first advances $\underline{\delta}$ by one time step using equation (9). The value of $\underline{p}_s$ at the forward step is obtained by parabolic extrapolation. With $\underline{\delta}$ and $\ddot{\underline{\delta}}$ at the forward point, equation (8) is then used to make the forward step for $\underline{p}_s$. Successive iterations are performed using the latest values of $\underline{p}_s$ and $\ddot{\underline{\delta}}$ on the right hand sides of equations (9) and (8).

Detailed information about this solution technique is given in reference [2].

D. MODEL PARAMETERS

The following parameters are used for structural response calculations.

Shell radius a	: 5 meters
Distance between bulkheads	: 16 meters
Shell thickness	: 0.05 meters
Circumferential average thickness	: 0.07 meters
Bulkhead thickness	: 0.02 meters
Structural material	: Steel
Yield stress for steel	: 700 Megapascals
Shell flexural rigidity ratio D_θ/D_z	: 100
Shell twisting rididity ratio $D_{\theta z}/D_z$	: 0.5

E. FAILURE CRITERIA

Failure criteria used by Newton and Atchison are employed. The following excerpt from reference [2] defines the basis.

> The largest calculated elastic stresses are found to be in the shell at the bulkhead. These stresses result from superposition of longitudinal bending and axial membrane compression. Since yielding at this location would not precipitate shell collapse, combinations of bending moment and axial force corresponding to failure are based on limit analysis (full yielding through thickness - part compression, remainder tension).
>
> A different situation exists at appreciable distances from the bulkhead. Here it is postulated that yielding will induce shell collapse. At such locations an effective uniaxial stress σ is calculated using the von Mises yield condition. Failure is deemed to occur when the utilization ratio $R = \sigma/\sigma_y$ reaches unity.

IV. RESULTS

A. INTRODUCTION

Results reported here concern two separate investigations. The first of these is a limited examination of the effectiveness of the radiation boundary condition. The second, and principal, study is a systematic examination of the effects of shock pulse rise time and duration on structural failure.

B. EFFECTIVENESS OF RADIATION BOUNDARY

The effectiveness of the radiation boundary condition is examined by repeated solutions of the same problem using successive reductions in the outside radius r_o of the fluid region. Table I gives the corresponding utilization ratios for both failure modes. The first line of the table provides the comparison standard, since the extreme values of the utilization ratios occur at 15.6 milliseconds and the time for an acoustic wave to travel from shell to the outer boundary and back is 18 milliseconds. The second line (r_o = 16.025 meters) also represents a case where the outer boundary is "far enough" from the shell so that the utilization ratios are unaltered. Succeeding radius reductions do affect the utilization ratios, but even for the smallest region (r_o = 8.15 meters) the ratios change by less than 3 percent. The accompanying reduction in the number of fluid nodes is dramatic. In reducing from r_o = 16.025 meters to r_o = 8.15 meters, the number of fluid nodes goes from 120 to 45.

TABLE I. Effect of Radiation Boundary Placement on Utilization Ratios

OUTSIDE RADIUS (METERS)	TRAVEL TIME (MS)	RELATIVE UTILIZATION RATIOS	
		LIMIT ANALYSIS	VON MISES
17.6	18.0	1.000	1.000
16.025	15.8	1.000	1.000
14.45	13.5	1.000	0.998
12.875	11.2	0.997	0.997
11.3	9.0	0.988	0.976
9.725	6.8	0.999	0.974
8.15	4.5	0.995	0.971

Notes:

1. Shell radius: a = 5 meters.
2. Cubic ramp-step wave with $c\tau_r/a = 0.97$.
3. Submergence pressure = 4.0 Megapascals,
   shock pressure = 4.5 Megapascals.
4. All maxima occur between 14.3 and 15.7 milliseconds after onset.
5. Travel time is time for acoustic wave to travel from shell to outer radius and back to shell (c = 1.4 meter/millisecond).

TABLE II. Effect of Fixed Outer Boundary Placement on Utilization Ratios

OUTSIDE RADIUS (METERS)	TRAVEL TIME (MS)	RELATIVE UTILIZATION RATIOS	
		LIMIT ANALYSIS	VON MISES
17.6	18.0	1.000	1.000
9.725	6.8	0.993	0.949
8.15	4.5	0.992	0.947

Notes: Notes for Table I apply here.

Table II exhibits the effect of reducing the outer radius of the region without imposing the radiation condition at that boundary. It is apparent that the resulting degradation of accuracy is more severe than with the radiation condition.

C. INFLUENCE OF PULSE RISE TIME AND DURATION ON STRUCTURE FAILURE

Considered here is the principal application of the improved analysis techniques introduced in this thesis. In reference [2] results were obtained for structural response to a cubic ramp-step shock wave. A single rise time $c\tau_r/a = 0.97$ was considered and the duration was effectively infinite. A large family of cubic ramp-box pulses is treated here. The rise time τ_r and effective duration $T = \frac{1}{2}\tau_r + \tau_d + \frac{1}{2}\tau_s$ are systematically varied. (Note that the impulse of the shock pulse is p*T. See Fig. 5.)

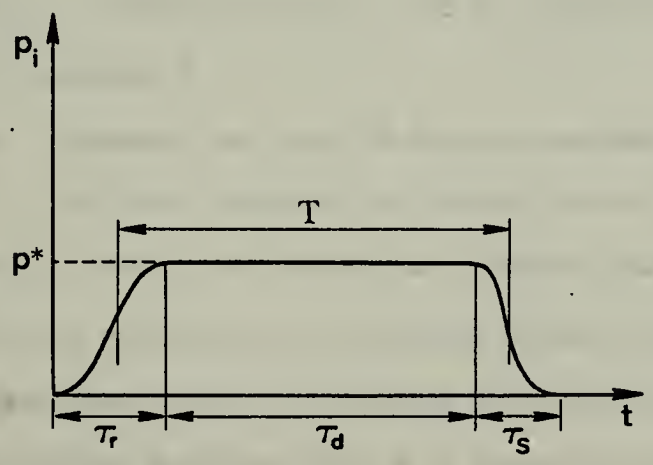

Fig. 5. Effective pulse duration T.

The pulse durations studied here are $cT/a = 2,4$, and 8. For each duration, four separate rise times: $c\tau_r/a = 0.1,0.2,0.4$, and 0.8 are considered. In every instance the fluid region extends from a = 5 meters to $r_o = 16.025$ meters. For all combinations with $c\tau_r/a > 0.1$ a

fluid mesh with 90 fluid elements and 120 fluid nodes is used ("coarse" mesh). The thickness (radial) of each element is 0.525 meters. With this mesh a time step h = 0.3 millisecond is used and the subsidence time is $c\tau_s/a = 0.2$. For the rise time $c\tau_r/a = 0.1$ a "fine" mesh is introduced with 174 fluid elements, 225 fluid nodes and a 0.2625 meter element thickness. With this mesh a time step h = 0.1 millisecond is used and the subsidence time is reduced to $c\tau_s/a = 0.1$.

For both meshes there are eight shell elements with lengths varying from 0.5 meters near the bulkhead to 2.0 meters midway between bulkheads. The number of structural degrees of freedom is 27 for each harmonic. Along the fluid-structure interface there is a fluid node coinciding with each structural node.

Results are presented graphically in the form of failure boundaries on the submergence pressure versus shock pressure plane in Figs. 6 through 17. Numerical results used to define these boundaries are tabulated in Appendix B.

Fig. 7 presents two sets of failure boundaries for $c\tau_r/a = 0.2$, $cT/a = 2$. For each boundary the narrow line is found using the fine mesh and the wide line is obtained from the coarse mesh.

When the effective pulse duration is small ($cT/a = 2$), changes in pulse rise time affect considerably the failure boundary. Increase in effective pulse duration ($cT/a \geq 4$) produces failure boundaries that are not sensitive to changes in rise time. In fact, for $cT/a = 8$ the same values are obtained for all rise times greater than $c\tau_r/a = 0.1$. It is considered that the small difference observed for $c\tau_r/a = 0.1$ is largely due to the mesh change. For durations greater than $cT/a = 4$ results approach those of Fig. 16, regardless of rise time. These results are

based on $c\tau_r/a = 0.97$ and $cT/a = \infty$, the pulse parameters used by Newton and Atchison [2]. The boundaries found here agree closely with those of reference [2], but it is noted that labels on ordinate and abscissa have been mistakenly interchanged on Fig. 10 of [2].

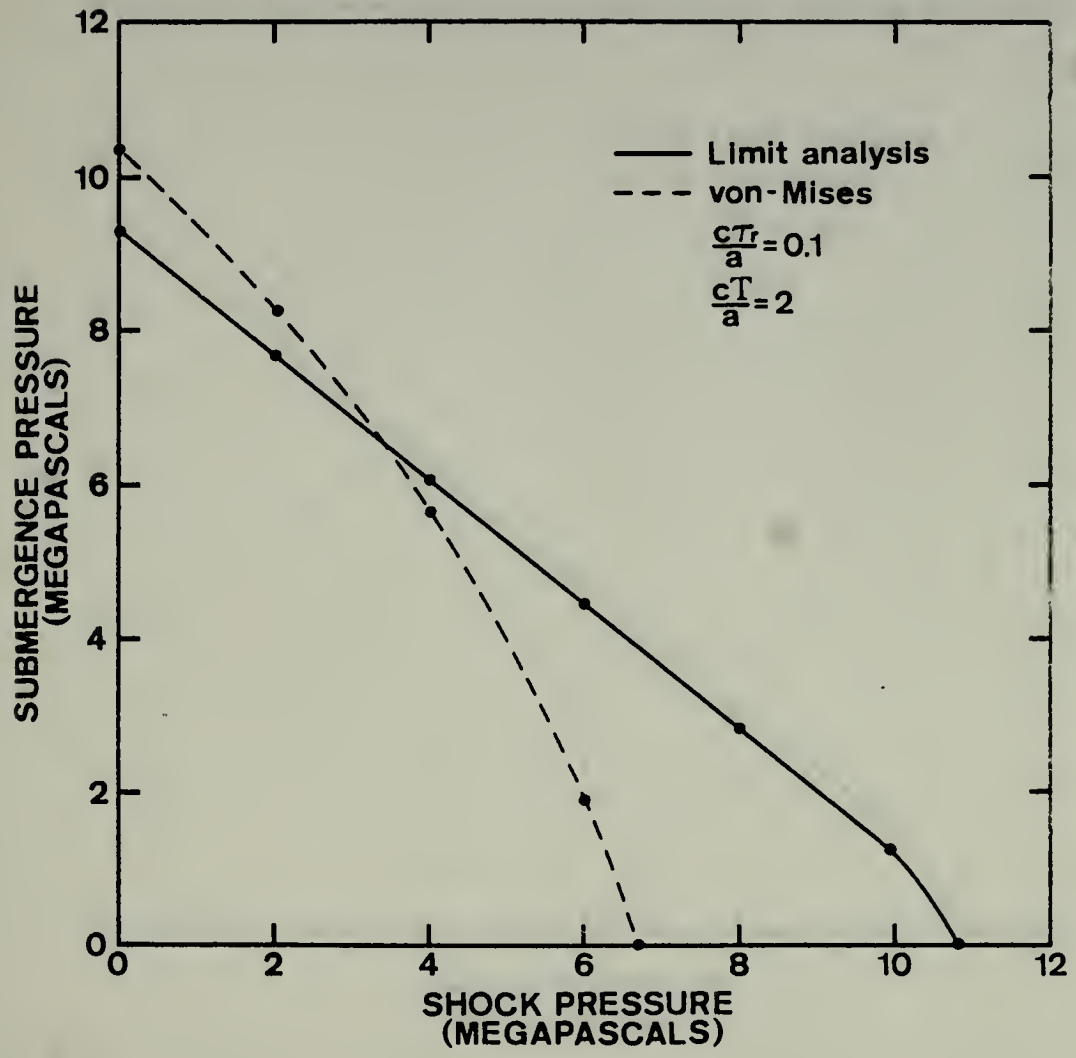

Fig. 6. Failure boundaries for $\frac{c\tau_r}{a} = 0.1$, $\frac{cT}{a} = 2$.

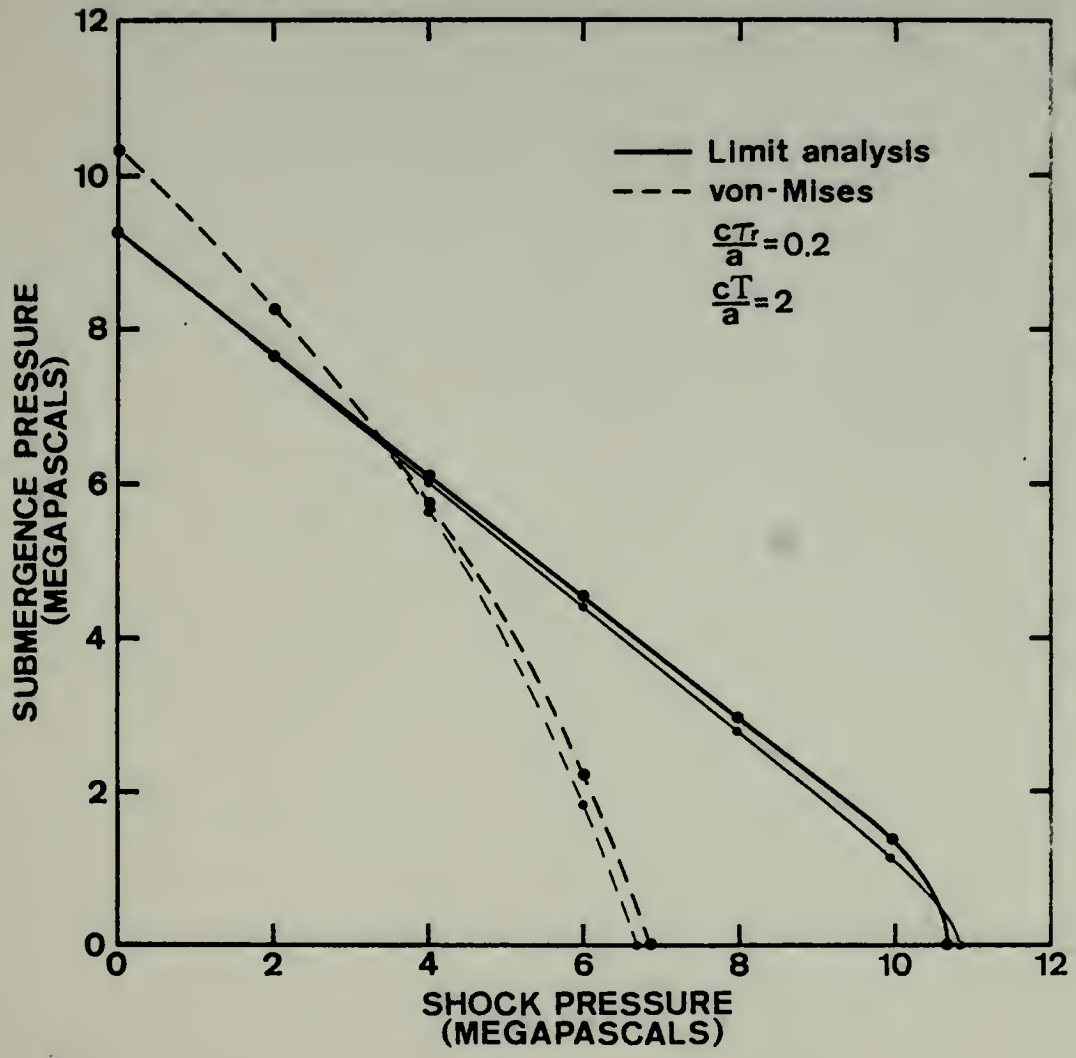

Fig. 7. Failure boundaries for $\frac{c\tau_r}{a} = 0.2$, $\frac{cT}{a} = 2$.

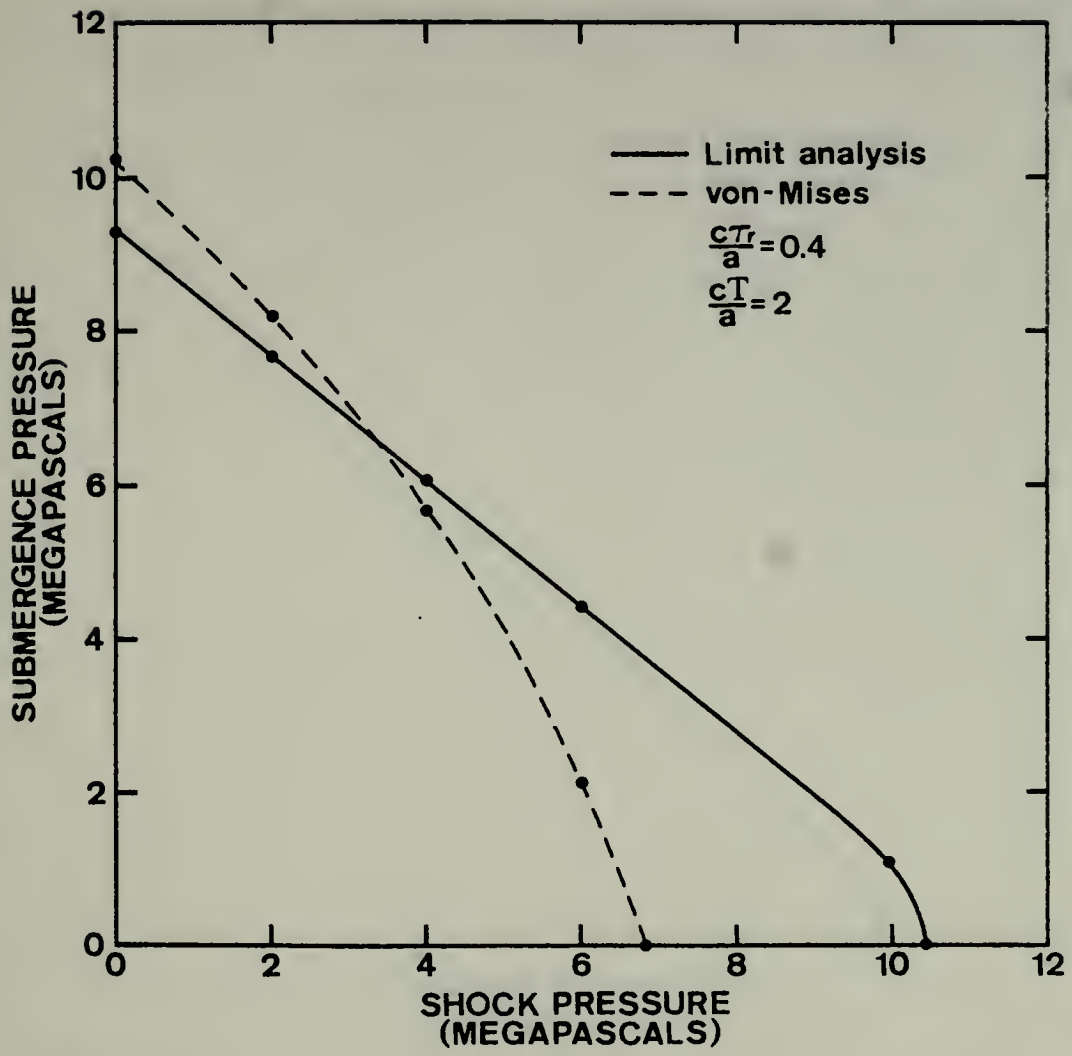

Fig. 8. Failure boundaries for $\frac{c\tau_r}{a} = 0.4$, $\frac{cT}{a} = 2$.

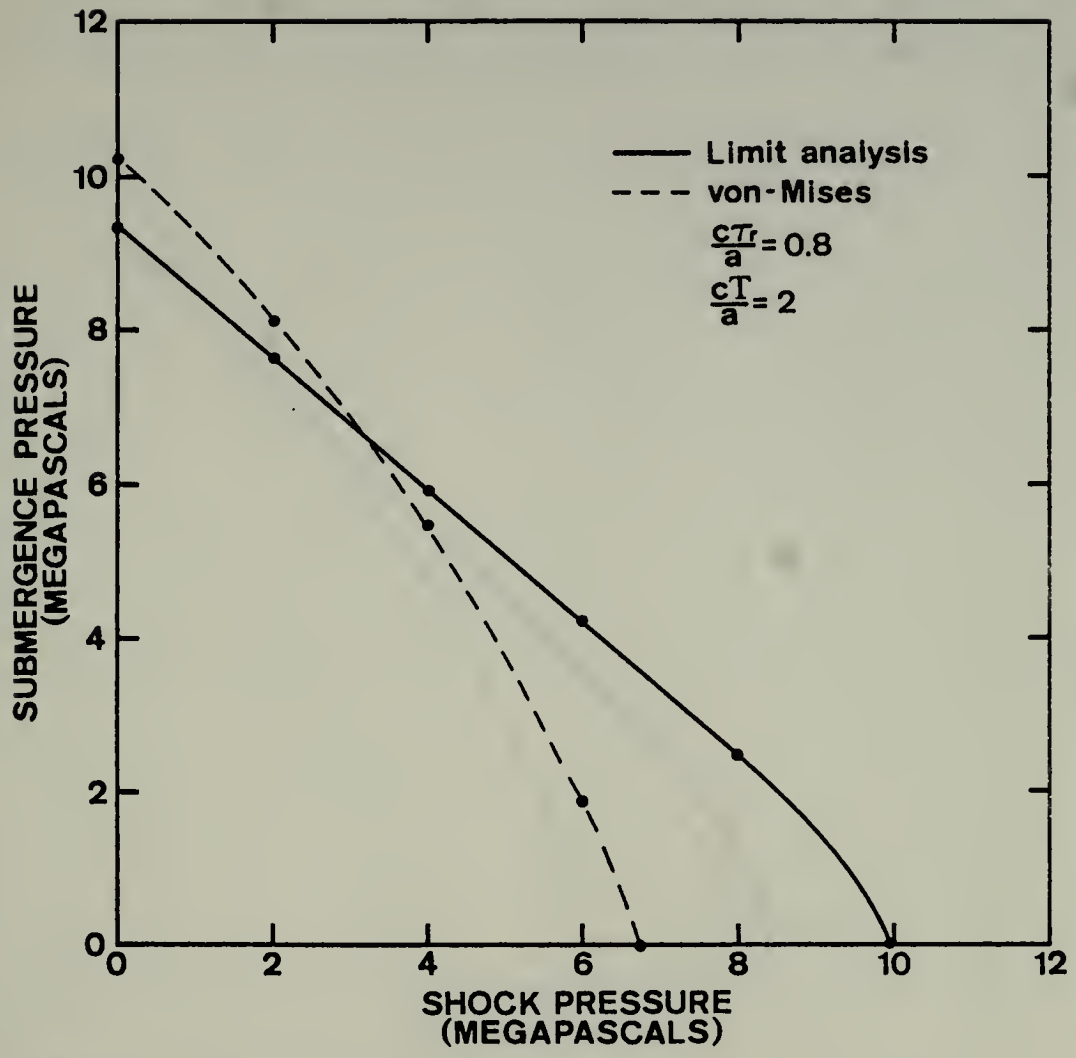

Fig. 9. Failure boundaries for $\frac{c\tau_r}{a} = 0.8$, $\frac{cT}{a} = 2$.

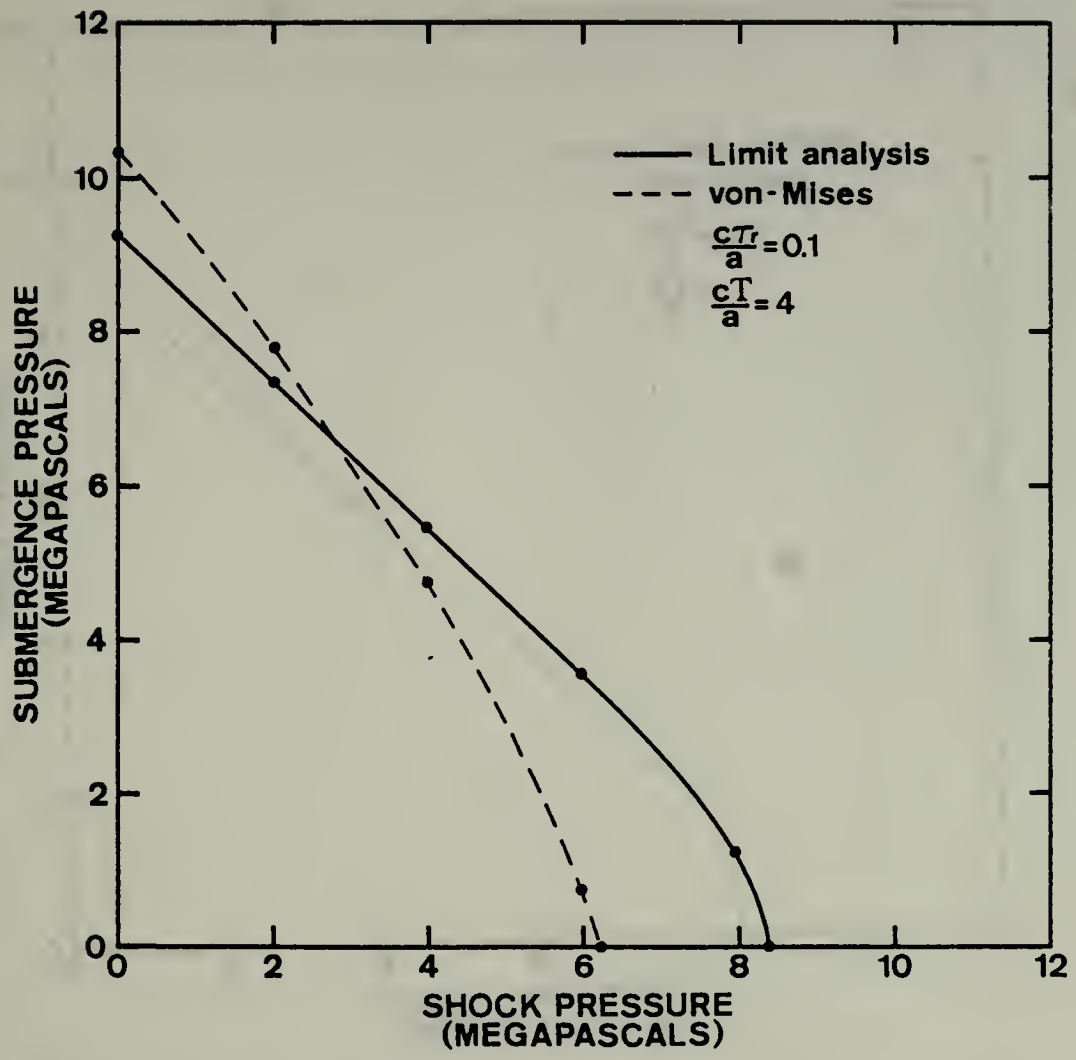

Fig. 10. Failure boundaries for $\frac{c\tau_r}{a} = 0.1$, $\frac{cT}{a} = 4$.

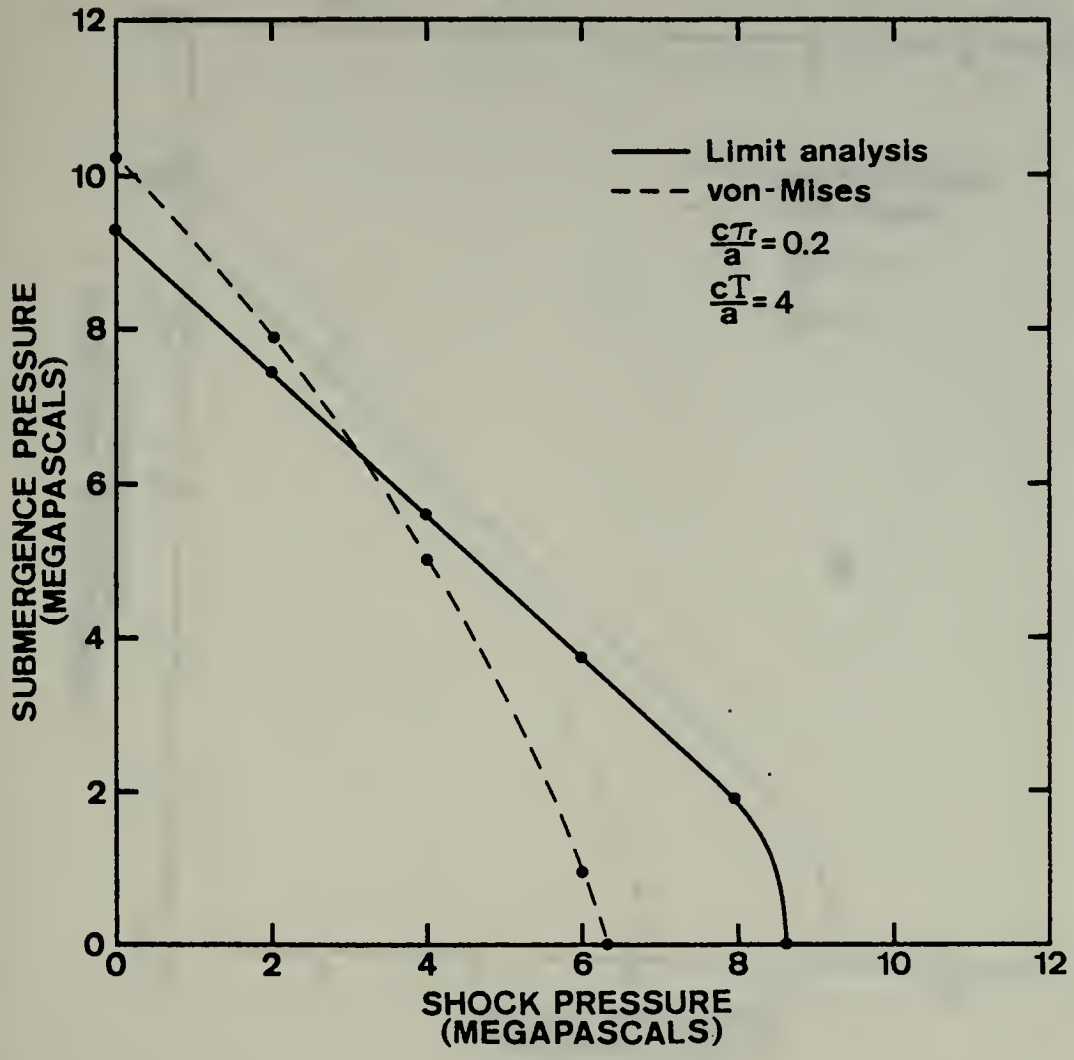

Fig. 11. Failure boundaries for $\frac{c\tau_r}{a} = 0.2$, $\frac{cT}{a} = 4$.

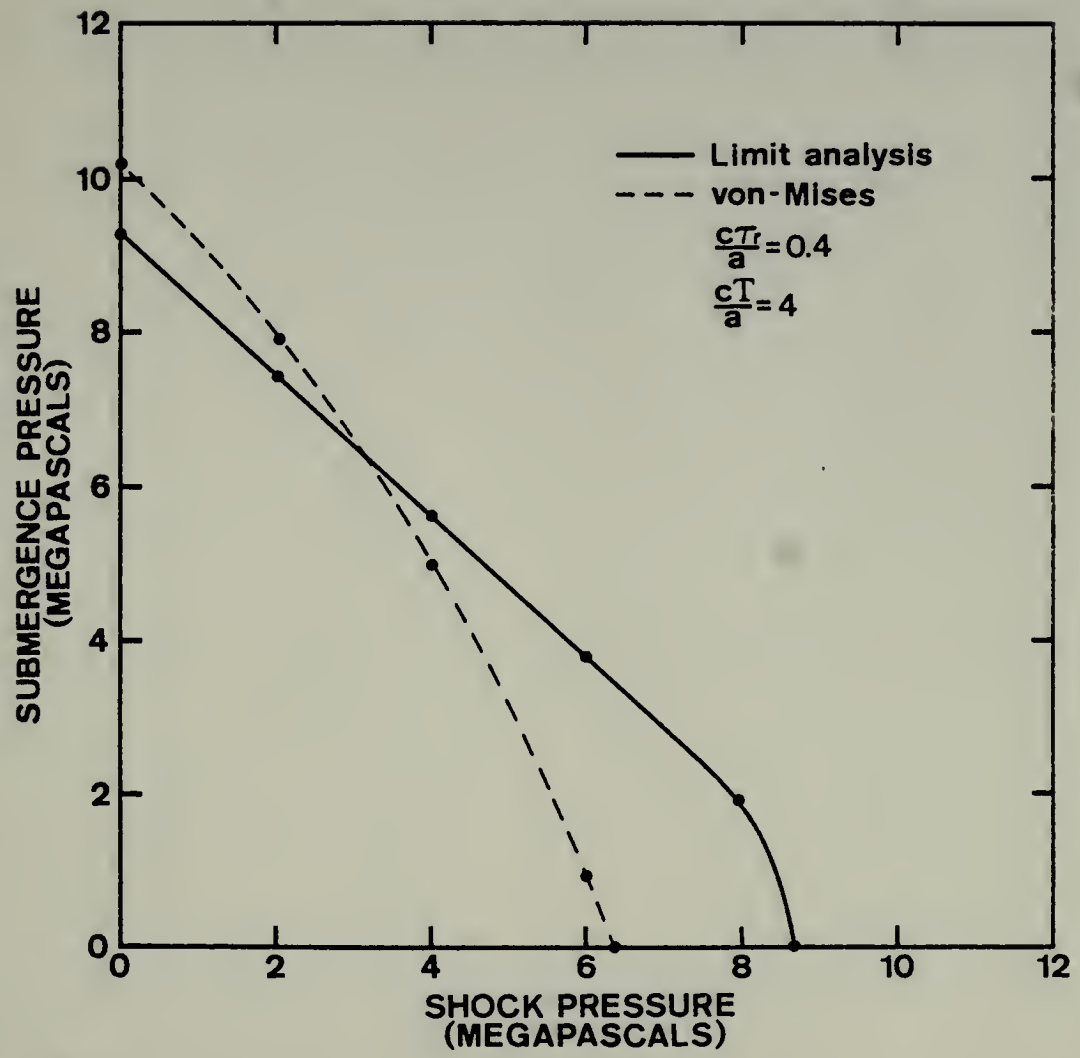

Fig. 12. Failure boundaries for $\frac{c\tau_r}{a} = 0.4$, $\frac{cT}{a} = 4$.

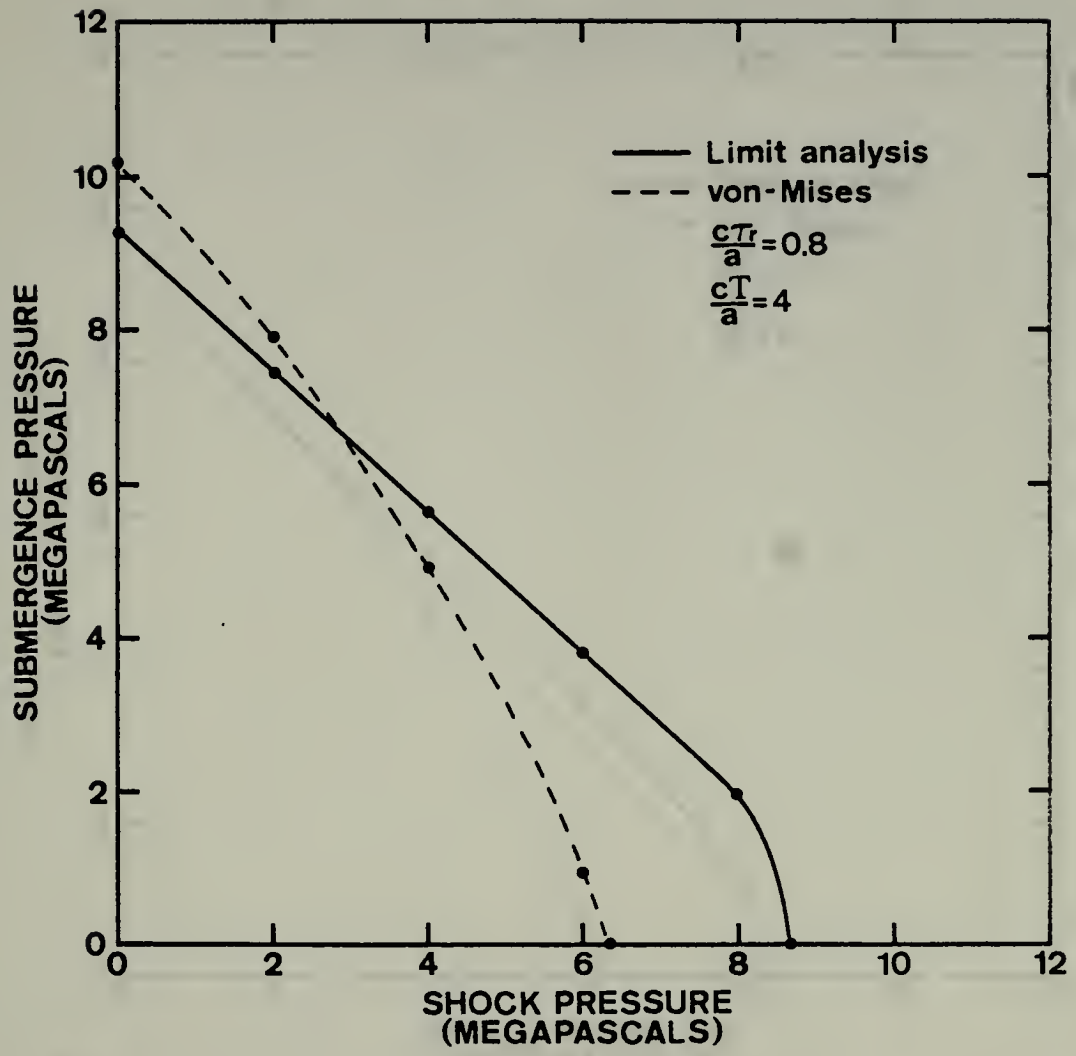

Fig. 13. Failure boundaries for $\frac{c\tau_r}{a} = 0.8$, $\frac{cT}{a} = 4$.

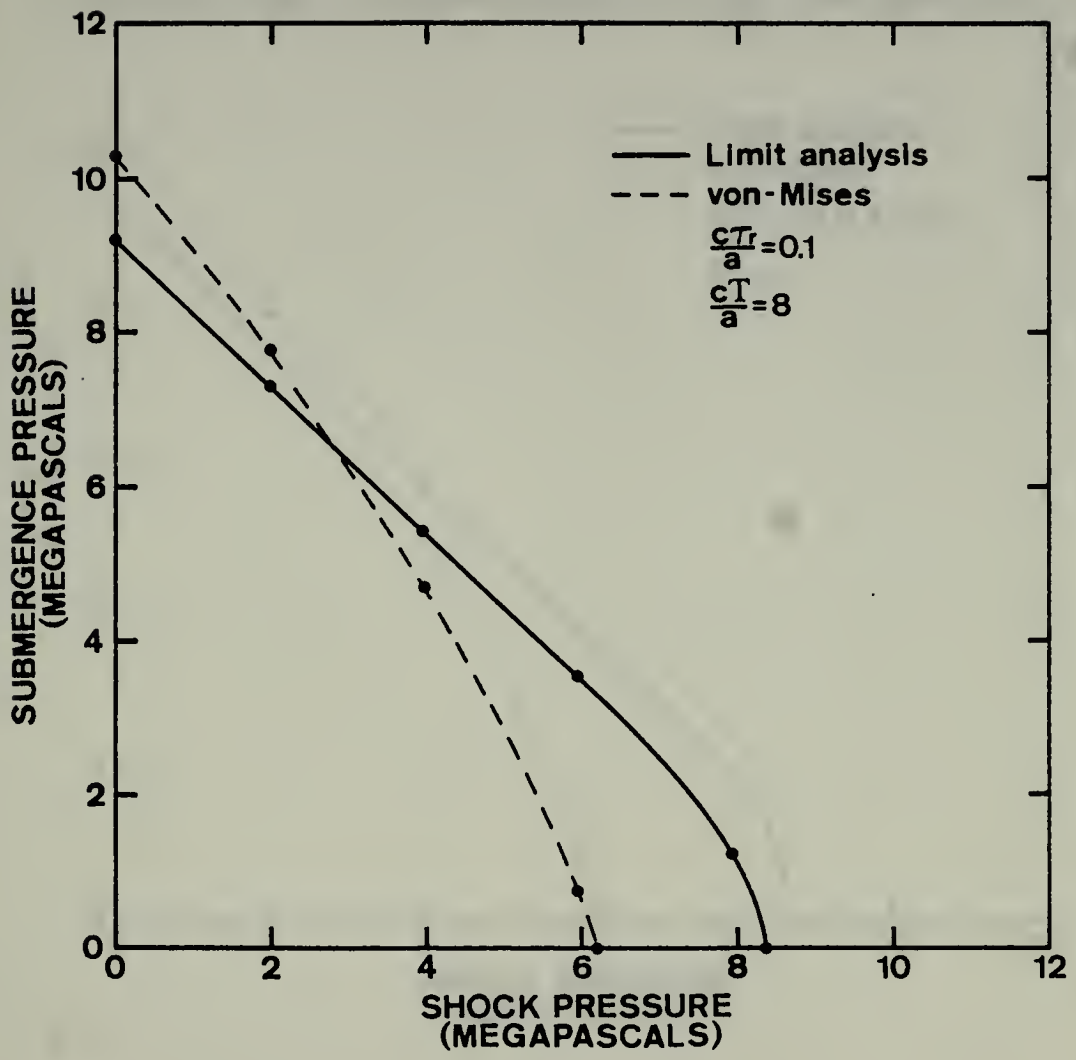

Fig. 14. Failure boundaries for $\frac{c\tau_r}{a} = 0.1$, $\frac{cT}{a} = 8$.

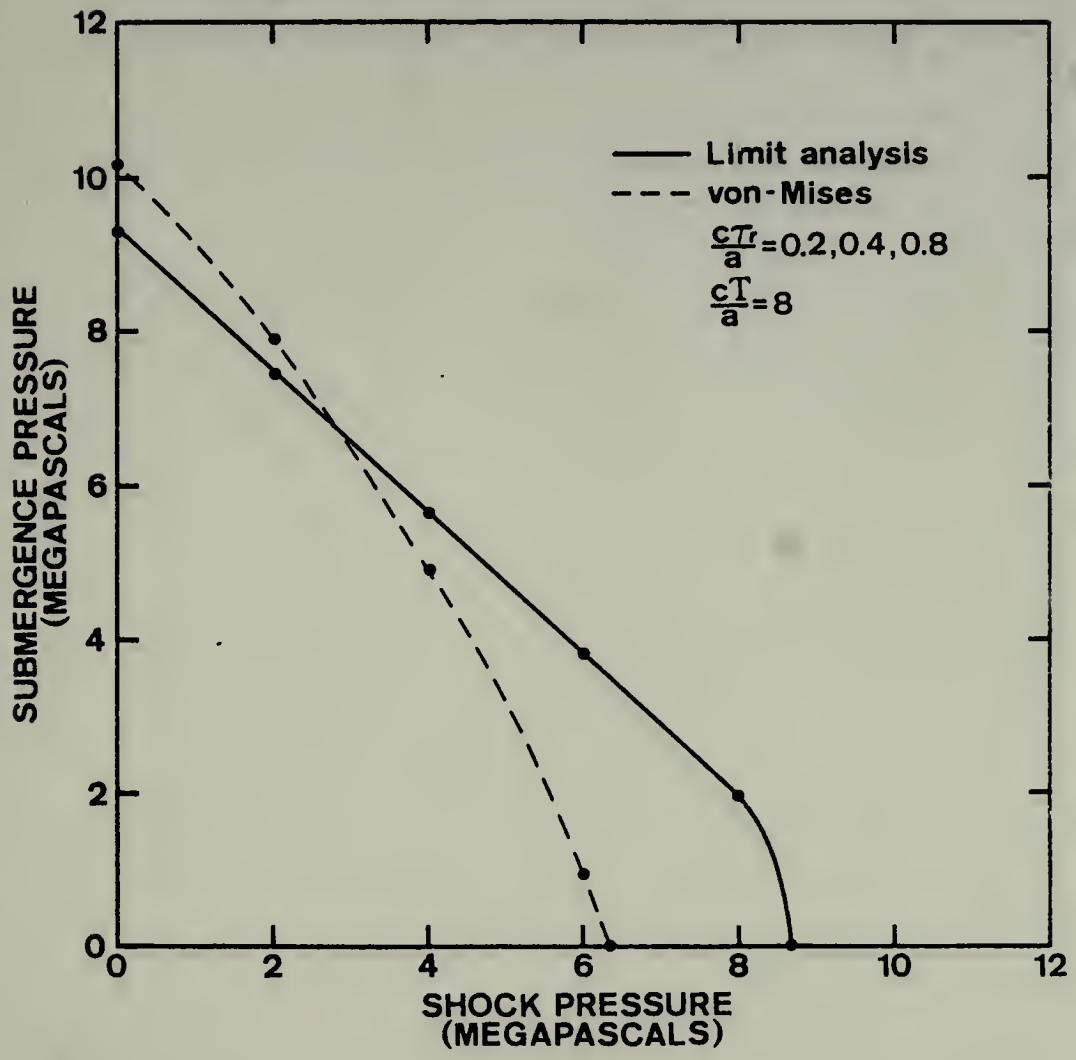

Fig. 15. Failure boundaries for $\frac{c\tau_r}{a}$ = 0.2,0.4,0.8; $\frac{cT}{a}$ = 8.

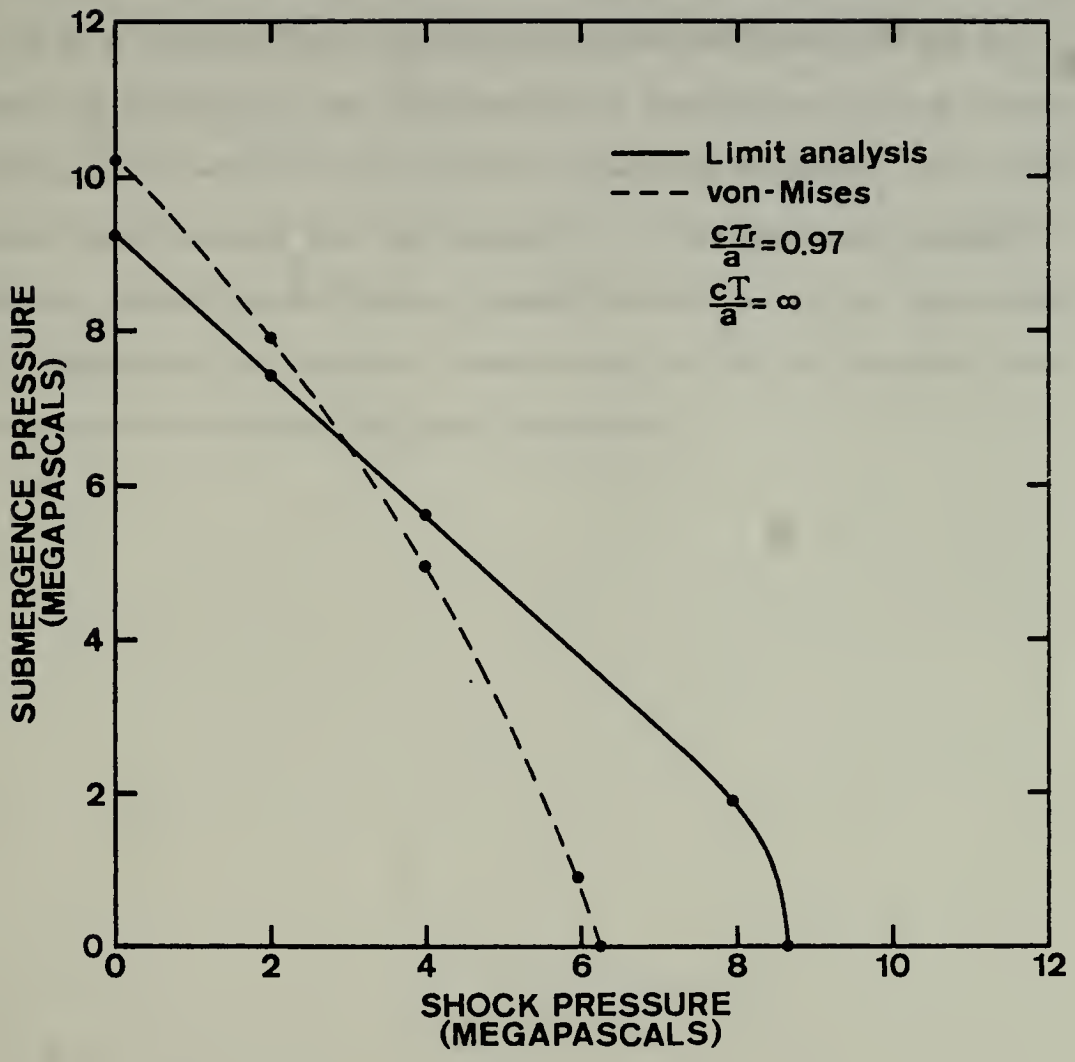

Fig. 16. Failure boundaries for $\frac{c\tau_r}{a} = 0.97$, $\frac{cT}{a} = \infty$.

V. CONCLUSIONS

It is concluded that the separation of the total dynamic pressure acting on a structure into incident and scattered pressures has improved the analysis of the fluid-structure interaction problem investigated in this thesis by avoiding the propagation solution. The results obtained also confirm that the imposition of the radiation boundary condition at the cylindric outer boundary affords a further improvement. For a representative structure, the effects on failure of pulse rise time and pulse duration have been established.

APPENDIX A. FLUID COEFFICIENT MATRICES

1. Separation of fluid equations

The governing equation for the scattered pressure is

$$\underline{Q}\,\ddot{\underline{p}} + \underline{D}\,\dot{\underline{p}} + \underline{H}\,\underline{p} = \rho\,\underline{L}^T\,\ddot{\underline{\delta}} - \underline{f} \tag{8}$$

where $\underline{p}$ is the vector of nodal scattered pressures. It is assumed that the (scattered) pressure p at a point (r, θ, z) of the fluid is given by

$$p = N_i\, p_{in} \cos n\theta \tag{A1}$$

where N_i, a function of r and z, is the shape function associated with fluid node i and p_{in} is the nth Fourier component of pressure at that node. Summation on indices i and n is implied.

This leads to a separate equation like equation 8 for each Fourier component of vector $\underline{p}$. The typical equation may be written as

$$\underline{Q}_n\,\ddot{\underline{p}}_n + \underline{D}_n\,\dot{\underline{p}}_n + \underline{H}_n\,\underline{p}_n = \rho\,\underline{L}_n^T\,\ddot{\underline{\delta}}_n - \underline{f}_n \tag{A2}$$

where the summation convention does not apply. Equation A2 assumes that Fourier resolution has also been applied to the structural nodal displacements and that the normal displacement w of the shell is given by

$$w = N_i'\,\delta_{in} \cos n\theta \tag{A3}$$

where N_i' , a function of z , is the shape function for structural node i and δ_{in} is the nth Fourier component of displacement at this node. As in equation (A1) the summation on i and n applies.

2. Formulas for matrix elements

Coefficient matrices are found by calculating contributions at the element level and assembling by addition. Presented in this section are the element-level contributions based on the convention that a lower case letter represents an element of the matrix denoted by the corresponding capital letter. Thus, q_{ijn} is the element in row i, column j, of matrix Q_n.

In each of the following formulas a symbol ε_n , the Neumann factor, appears. It is defined to have the value 1 for n=0 and the value 2 for n any positive integer. In the two following formulas the integrations with respect to r and z extend over the range for the individual fluid element.

$$q_{ijn} = \frac{2\pi}{\varepsilon_n c^2} \iint N_i \, N_j \, r \, dr \, dz \qquad \text{(A4)}$$

$$h_{ijn} = \frac{2\pi}{\varepsilon_n} \iint \left(\frac{\partial N_i}{\partial r} \frac{\partial N_j}{\partial r} + \frac{\partial N_i}{\partial z} \frac{\partial N_j}{\partial z} + \frac{n^2}{r^2} N_i \, N_j \right) r \, dr \, dz \qquad \text{(A5)}$$

No summation on n is intended in equation (A5).

The following two formulas concern the boundary condition at the structure-fluid interface (r=a). The only fluid nodes having non-zero contributions are those in contact with the shell. Integrations with respect to z take place along a structural element and the matching fluid element.

$$\ell_{ijn} = \frac{2\pi a}{\varepsilon_n} \int N_i' N_j \, dz \qquad \text{(A6)}$$

$$b_{jn} = \frac{2\pi a}{\varepsilon_n} \int N_j \, dz \qquad \text{(A7)}$$

The component b_{jn}, when multiplied by B_n as defined in equation (23), gives the jth component of vector $-\underline{f}_n$.

The final two formulas represent contributions due to the radiation boundary condition applied at the outer boundary ($r = r_o$). Integration with respect to z is carried out along that boundary. Only fluid nodes on that boundary are included

$$d_{ijn} = \frac{2\pi r_o}{c\varepsilon_n} \int N_i N_j \, dz \qquad \text{(A8)}$$

$$\Delta h_{ijn} = \frac{\pi}{\varepsilon_n} \int N_i N_j \, dz \qquad \text{(A9)}$$

The contributions Δh_{ijn} are assembled into $\underline{H}_n$.

APPENDIX B

NUMERICAL RESULTS FOR FAILURE BOUNDARIES

FAILURE BOUNDARY VALUES

$\frac{c\tau_r}{a} = 0.1$

$\frac{c\tau}{a} = 2$

Number of fluid elements: 174

LIMIT ANALYSIS

SHOCK PRESSURE (MEGAPASCALS)	SUBMERGENCE PRES. (MEGAPASCALS)	MAXIMUM RATIO	TIME MAXIMUM RATIO (MILLISECONDS)
0.00	9.27	0.999	
2.00	7.67	1.001	9.6
4.00	6.04	1.000	9.6
6.00	4.41	0.999	9.6
8.00	2.79	1.000	9.6
10.00	1.15	1.000	9.6
10.84	0.0	1.000	9.6

von-Mises

SHOCK PRESSURE (MEGAPASCALS)	SUBMERGENCE PRES. (MEGAPASCALS)	MAXIMUM RATIO	TIME MAXIMUM RATIO (MILLISECONDS)
0.00	10.20	1.001	
2.00	8.28	0.999	10.2
4.00	5.64	1.001	10.2
6.00	1.84	1.000	10.2
6.70	0.0	1.000	10.2

FAILURE BOUNDARY VALUES

$\frac{c\tau_r}{a} = 0.2$

$\frac{c\tau}{a} = 2$

Number of fluid elements: 90

LIMIT ANALYSIS

SHOCK PRESSURE (MEGAPASCALS)	SUBMERGENCE PRES. (MEGAPASCALS)	MAXIMUM RATIO	TIME MAXIMUM RATIO (MILLISECONDS)
0.00	9.27	0.999	
2.00	7.71	1.000	9.6
4.00	6.13	1.000	9.6
6.00	4.55	1.000	9.6
8.00	2.96	1.000	9.6
10.00	1.37	1.000	9.6
10.74	0.00	0.999	9.6

von-Mises

SHOCK PRESSURE (MEGAPASCALS)	SUBMERGENCE PRES. (MEGAPASCALS)	MAXIMUM RATIO	TIME MAXIMUM RATIO (MILLISECONDS)
0.00	10.20	1.001	
2.00	8.30	1.000	10.8
4.00	5.75	1.001	10.8
6.00	2.20	1.000	10.8
6.89	0.00	1.000	10.8

FAILURE BOUNDARY VALUES

$\frac{c\tau_r}{a} = 0.2$

$\frac{c\tau}{a} = 2$

Number of fluid elements: 174

LIMIT ANALYSIS

SHOCK PRESSURE (MEGAPASCALS)	SUBMERGENCE PRES. (MEGAPASCALS)	MAXIMUM RATIO	TIME MAXIMUM RATIO (MILLISECONDS)
0.00	9.27	0.999	
2.00	7.65	1.000	9.6
4.00	6.03	1.000	9.6
6.00	4.40	1.000	9.6
8.00	2.76	1.000	9.6
10.00	1.12	1.000	9.6
10.84	0.00	1.000	9.6

von-Mises

SHOCK PRESSURE (MEGAPASCALS)	SUBMERGENCE PRES. (MEGAPASCALS)	MAXIMUM RATIO	TIME MAXIMUM RATIO (MILLISECONDS)
0.00	10.20	1.001	
2.00	8.29	1.000	10.2
4.00	5.65	1.000	10.2, 10.8
6.00	1.84	1.000	10.8
6.89	0.00	1.000	10.8

FAILURE BOUNDARY VALUES

$\frac{cT_r}{a} = 0.4$

$\frac{cT}{a} = 2$

Number of fluid elements: 90

LIMIT ANALYSIS

SHOCK PRESSURE (MEGAPASCALS)	SUBMERGENCE PRES. (MEGAPASCALS)	MAXIMUM RATIO	TIME MAXIMUM RATIO (MILLISECONDS)
0.00	9.27	0.999	
2.00	7.66	0.999	10.8
4.00	6.05	1.000	10.8
6.00	4.43	1.000	10.8
8.00	2.80	1.000	10.8
10.00	1.04	1.000	10.8
10.44	0.00	1.000	10.8

von-Mises

SHOCK PRESSURE (MEGAPASCALS)	SUBMERGENCE PRES. (MEGAPASCALS)	MAXIMUM RATIO	TIME MAXIMUM RATIO (MILLISECONDS)
0.00	10.20	1.001	
2.00	8.26	1.000	10.8
4.00	5.63	1.000	10.8
6.00	2.14	1.000	10.8
6.86	0.00	1.000	10.8

FAILURE BOUNDARY VALUES

$\frac{c\tau_r}{a} = 0.8$

$\frac{cT}{a} = 2$

Number of fluid elements: 90

LIMIT ANALYSIS

SHOCK PRESSURE (MEGAPASCALS)	SUBMERGENCE PRES. (MEGAPASCALS)	MAXIMUM RATIO	TIME MAXIMUM RATIO (MILLISECONDS)
0.00	9.27	0.999	
2.00	7.63	1.001	12.0
4.00	5.96	1.000	12.0
6.00	4.30	1.000	12.0
8.00	2.48	1.000	12.0
10.00	0.00	1.002	12.0

von-Mises

SHOCK PRESSURE (MEGAPASCALS)	SUBMERGENCE PRES. (MEGAPASCALS)	MAXIMUM RATIO	TIME MAXIMUM RATIO (MILLISECONDS)
0.00	10.20	1.001	
2.00	8.17	1.000	12.0
4.00	5.50	1.000	12.0
6.00	1.86	1.001	12.0
6.76	0.00	0.999	12.0

FAILURE BOUNDARY VALUES

$\frac{c\tau_r}{a} = 0.1$

$\frac{cT}{a} = 4$

Number of fluid elements: 174

LIMIT ANALYSIS

SHOCK PRESSURE (MEGAPASCALS)	SUBMERGENCE PRES. (MEGAPASCALS)	MAXIMUM RATIO	TIME MAXIMUM RATIO (MILLISECONDS)
0.00	9.27	0.999	
2.00	7.37	1.000	12.6
4.00	5.46	1.000	12.6
6.00	3.55	1.000	12.6
8.00	1.26	1.000	12.6
8.38	0.00	1.000	12.6

von-Mises

SHOCK PRESSURE (MEGAPASCALS)	SUBMERGENCE PRES. (MEGAPASCALS)	MAXIMUM RATIO	TIME MAXIMUM RATIO (MILLISECONDS)
0.00	10.20	1.001	
2.00	7.81	1.001	12.6
4.00	4.78	1.000	12.6, 13.2
6.00	0.78	1.003	13.2
6.08	0.00	1.000	13.2

FAILURE BOUNDARY VALUES

$\frac{cT_r}{a} = 0.2$

$\frac{cT}{a} = 4$

Number of fluid elements: 90

LIMIT ANALYSIS

SHOCK PRESSURE (MEGAPASCALS)	SUBMERGENCE PRES. (MEGAPASCALS)	MAXIMUM RATIO	TIME MAXIMUM RATIO (MILLISECONDS)
0.00	9.27	0.999	
2.00	7.44	1.000	13.2
4.00	5.59	1.000	13.2
6.00	3.74	1.000	13.2
8.00	1.92	1.003	13.2
8.65	0.00	1.001	13.2

von-Mises

SHOCK PRESSURE (MEGAPASCALS)	SUBMERGENCE PRES. (MEGAPASCALS)	MAXIMUM RATIO	TIME MAXIMUM RATIO (MILLISECONDS)
0.00	10.20	1.001	
2.00	7.90	1.001	13.2
4.00	4.90	1.000	13.2
6.00	0.90	1.000	13.2
6.35	0.00	1.000	13.2

FAILURE BOUNDARY VALUES

$\frac{c\tau_r}{a} = 0.4$

$\frac{cT}{a} = 4$

Number of fluid elements: 90

LIMIT ANALYSIS

SHOCK PRESSURE (MEGAPASCALS)	SUBMERGENCE PRES. (MEGAPASCALS)	MAXIMUM RATIO	TIME MAXIMUM RATIO (MILLISECONDS)
0.00	9.27	0.999	
2.00	7.44	1.000	13.2, 14.4
4.00	5.60	1.000	13.2, 14.4
6.00	3.76	1.000	13.2, 14.4
8.00	1.92	1.001	13.2, 14.4
8.69	0.00	1.000	13.2, 14.4

von-Mises

SHOCK PRESSURE (MEGAPASCALS)	SUBMERGENCE PRES. (MEGAPASCALS)	MAXIMUM RATIO	TIME MAXIMUM RATIO (MILLISECONDS)
0.00	10.20	1.000	
2.00	7.90	1.000	13.2, 14.4
4.00	4.94	1.001	14.4
6.00	0.90	1.001	14.4
6.35	0.00	1.000	14.4

FAILURE BOUNDARY VALUES

$\frac{c\tau_r}{a} = 0.8$

$\frac{cT}{a} = 4$

Number of fluid elements: 90

LIMIT ANALYSIS

SHOCK PRESSURE (MEGAPASCALS)	SUBMERGENCE PRES. (MEGAPASCALS)	MAXIMUM RATIO	TIME MAXIMUM RATIO (MILLISECONDS)
0.00	9.27	0.999	
2.00	7.44	1.000	14.4
4.00	5.60	1.000	14.4
6.00	3.76	1.000	14.4
8.00	1.91	0.999	14.4
8.69	0.00	1.000	14.4

von-Mises

SHOCK PRESSURE (MEGAPASCALS)	SUBMERGENCE PRES. (MEGAPASCALS)	MAXIMUM RATIO	TIME MAXIMUM RATIO (MILLISECONDS)
0.00	10.20	1.001	
2.00	7.90	1.000	14.4
4.00	4.94	1.001	14.4
6.00	0.90	0.999	14.4
6.35	0.00	0.997	14.4

FAILURE BOUNDARY VALUES

$\frac{c\tau_r}{a} = 0.1$

$\frac{cT}{a} = 8$

Number of fluid elements: 174

LIMIT ANALYSIS

SHOCK PRESSURE (MEGAPASCALS)	SUBMERGENCE PRES. (MEGAPASCALS)	MAXIMUM RATIO	TIME MAXIMUM RATIO (MILLISECONDS)
0.00	9.27	0.999	
2.00	7.37	1.000	12.6
4.00	5.46	1.000	12.6
6.00	3.55	1.000	12.6
8.00	1.26	1.000	12.6
8.38	0.00	1.000	12.6

von-Mises

SHOCK PRESSURE (MEGAPASCALS)	SUBMERGENCE PRES. (MEGAPASCALS)	MAXIMUM RATIO	TIME MAXIMUM RATIO (MILLISECONDS)
0.00	10.20	1.001	
2.00	7.81	1.001	12.6
4.00	4.78	1.000	12.6, 13.2
6.00	0.78	1.003	13.2
6.08	0.00	1.000	13.2

FAILURE BOUNDARY VALUES

$\frac{c\tau_r}{a} = 0.2,\ 0.4,\ 0.8$

$\frac{cT}{a} = 8$

Number of fluid elements: 90

LIMIT ANALYSIS

SHOCK PRESSURE (MEGAPASCALS)	SUBMERGENCE PRES. (MEGAPASCALS)	MAXIMUM RATIO	TIME MAXIMUM RATIO (MILLISECONDS)
0.00	9.27	0.999	
2.00	7.44	1.000	13.2
4.00	5.59	1.000	13.2
6.00	3.74	1.000	13.2
8.00	1.92	1.003	13.2
8.65	0.00	1.001	13.2

von-Mises

SHOCK PRESSURE (MEGAPASCALS)	SUBMERGENCE PRES. (MEGAPASCALS)	MAXIMUM RATIO	TIME MAXIMUM RATIO (MILLISECONDS)
0.00	10.20	1.001	
2.00	7.90	1.001	13.2
4.00	4.90	1.000	13.2
6.00	0.90	1.000	13.2
6.35	0.00	1.000	13.2

FAILURE BOUNDARY VALUES

$\frac{c\tau_r}{a} = 0.97$

$\frac{cT}{a} = \infty$

Number of fluid elements: 102

LIMIT ANALYSIS

SHOCK PRESSURE (MEGAPASCALS)	SUBMERGENCE PRES. (MEGAPASCALS)	MAXIMUM RATIO	TIME MAXIMUM RATIO (MILLISECONDS)
0.00	9.27	0.999	
2.00	7.45	1.000	14.4, 15.6
4.00	5.62	1.000	14.4, 15.6
6.00	3.75	1.000	14.4
8.00	1.95	1.000	14.4
8.70	0.00	0.998	14.4

von-Mises

SHOCK PRESSURE (MEGAPASCALS)	SUBMERGENCE PRES. (MEGAPASCALS)	MAXIMUM RATIO	TIME MAXIMUM RATIO (MILLISECONDS)
0.00	10.20	1.001	
2.00	7.91	1.000	14.4
4.00	4.95	1.000	14.4
6.00	0.94	1.000	15.6

LIST OF REFERENCES

1. Atchison, D. L.: "Finite element solution of the interaction of a plane acoustic blast wave and a cylindric structure," Thesis, Naval Postgraduate School, June 1974.

2. Newton, R. E. and Atchison, D. L.: "Response of a ring-stiffened cylinder to an acoustic blast wave," Second International Symposium on Finite Element Methods in Flow Problems, S. Margherita Ligure, Italy, June 1976.

3. Mindlin, R. D. and Bleich, H. H.: "Response of an elastic cylindrical shell to a transverse, step shock wave," J. Appl. Mech., Vol. 20, p. 189, 1953.

4. Geers, T. L.: "Transient response analysis of submerged structures," in Finite Element Analysis of Transient Nonlinear Structural Behavior, T. Belytschko, J. R. Osios and P. V. Marcal, eds., AMD-Vol 14, A.S.M.E., 1975.

5. Everstine, G. C.: "A NASTRAN implementation of the doubly asymptotic approximation for underwater shock response," Proceedings of fifth NASTRAN users colloquium, Moffett Field, CA., October 1976.

6. Zienkiewicz, O. C. and Newton, R. E." "Coupled vibrations of a structure submerged in a compressible fluid," International Symposium on finite element techniques, Stuttgart, 1969.

7. Chenault, D. W., II: "Motion of a ship at the free surface," M.S. Thesis, Naval Postgraduate School, 1970.

8. Dean, D. V.: "Finite element study of acoustic waves," M.S. Thesis, Naval Postgraduate School, 1970.

9. Bai, K. J.: "A variational method in potential flows with a free surface," Report No. NA72-2, University of California, Berkeley, College of Engineering, 1972.

10. Houbolt, J. C.: "A recurrence matrix solution for the dynamic response of elastic aircraft," J. Aero. Sci., Vol 17, No. 9, (Sept. 1950), 540-550.

11. Grafton, P. E. and Strome, D. R.: "Analysis of axisymmetric shells by the direct stiffness method," AIAA J., 2342-7, 1963.

INITIAL DISTRIBUTION LIST

		No. Copies
1.	Defense Documentation Center Cameron Station Alexandria, Virginia 22314	2
2.	Library, Code 0142 Naval Postgraduate School Monterey, California 93940	2
3.	Department Chairman, Code 69 Department of Mechanical Engineering Naval Postgraduate School Monterey, California 93940	2
4.	Professor R. E. Newton, Code 69Ne Department of Mechanical Engineering Naval Postgraduate School Monterey, California 93940	4
5.	Lt. Jose G. Gallo, Peruvian Navy Las Magnolias 203 Lima 4, Peru	1
6.	Dr. Eugene Sevin SPSS Defense Nuclear Agency Washington, D. C. 20305	1
7.	Dr. Gordon C. Everstine, Code 1844 David W. Taylor Naval Ship Research and Development Center Bethesda, Maryland 20084	1
8.	Dr. Nicholas L. Basdekas, Code 474 Office of Naval Research Arlington, Virginia 22217	1
9.	Dr. Melvin L. Baron Weidlinger Associates 110 East 59th Street New York, New York 10022	1
10.	Dr. Thomas L. Geers Dept. 52-33/Bldg. 205 Lockheed Palo Alto Research Laboratory 3251 Hanover Street Palo Alto, California 94304	1

Thesis 174750
G14065 Gallo
c.1 Shock induced struc-
tural response.